

# The Luminosity Function of Nearby Galaxy Clusters II: Redshifts and Luminosity Function for Galaxies in the Region of the Centaurus Cluster

Kristin Chiboucas<sup>1</sup>

*Gemini Observatory*

*670 N. A'ohoku Pl, Hilo, HI 96720-2700*

kchibouc@gemini.edu

and

Mario Mateo

*University of Michigan*

*Department of Astronomy, Univ. of Michigan, Ann Arbor, MI 48109-1090*

mmateo@umich.edu

## ABSTRACT

We acquired spectra for a random sample of galaxies within a 0.83 square degree region centered on the core of the Centaurus cluster. Radial velocities were obtained for 225 galaxies to limiting magnitudes of  $V < 19.5$ . Of the galaxies for which velocities were obtained, we find 35% to be member galaxies. New redshifts are obtained for 15 Centaurus cluster members, many of these dwarf galaxies. Radial velocities for the other members agree well with those from previous studies. Of the 78 member galaxies, magnitudes range from  $11.8 < V < 18.5$  ( $-21.6 < M_V < -14.9$  for  $H_0 = 70 \text{ km s}^{-1} \text{ Mpc}^{-1}$ ) with a limiting central surface brightness of  $\mu_0 < 22.5 \text{ mag arcsec}^{-2}$ . While many of these galaxies are giants, about 25 galaxies with  $M_V > -17.0$  are considered dwarfs. We constructed the cluster galaxy luminosity function by using these spectroscopic results to calculate the expected fraction of cluster members in each magnitude bin. The faint-end slope of the luminosity function using this method is shallower than the one obtained using a statistical method to correct for background galaxy

---

<sup>1</sup>Work done while at The University of Michigan

contamination. We also use the spectroscopy results to define surface brightness criteria to establish membership for the full sample. Using these criteria, we find a luminosity function very similar to the one constructed with the statistical background correction. For both, we find a faint-end slope  $\alpha \sim -1.4$ . The error in faint-end slope for the statistically corrected LF is  $\sim \pm 0.2$ . Adjusting the surface brightness membership criteria we find that the data are consistent with a faint-end slope as shallow as  $-1.22$  or as steep as  $-1.50$ . We describe in this paper some of the limitations of using these methods for constructing the galaxy luminosity function. This is paper II in our investigation of the cluster galaxy luminosity function.

*Subject headings:* galaxy clusters: individual Centaurus (A3526) - techniques: spectroscopic - galaxies: luminosity function - galaxies: emission lines - galaxies: absorption lines - galaxies: distances and redshifts - galaxies: dwarf

## 1. Introduction

There is a paucity of spectroscopic and kinematical information on dwarf galaxies in clusters. Most existing data comes from the nearby Virgo and Fornax clusters (see e.g. Conselice et al. (2001), Drinkwater et al. (2000), Pedraz et al. (2002), Geha et al. (2003), van Zee et al. (2004), Gavazzi et al. (2004)). Data also exist for Centaurus (Stein et al. (1997) and this work) and Coma (Edwards et al. (2002) and references therein). Even within these relatively nearby clusters, spectroscopy of dwarf galaxies is a challenging task, requiring spectra for (typically) low-surface brightness galaxies with integrated magnitudes as faint as  $R \sim 20$ , or  $B \sim 21$ .

Nonetheless, obtaining large kinematic samples of cluster dwarf galaxies is important for a number of reasons. Processes involved in cluster formation and evolution leave dynamical signatures on the velocity distribution of member galaxies. A comparison of the velocity distributions along with spatial distributions as a function of galaxy type provides important clues about the dynamical history of the clusters and of the different galaxy populations (Edwards et al. 2002). Several possible formation mechanisms for dwarf galaxies may be tested in this way. Dwarfs may have formed, for example, early on in the cluster, later from infalling spirals which are subjected to stripping/harassment, from the transformation of infalling dIrrs, or may instead originate from a population of satellites previously bound to infalling spirals. The velocity distribution and dispersion coupled with spatial distributions will indicate whether the population is highly clustered and virialized, or has a larger spread indicative of infall or substructure. The few studies of cluster kinematics in Fornax, Virgo,

Coma, and Centaurus have revealed evidence for a number of these formation mechanisms and hint at different evolutionary scenarios for the clusters (Drinkwater et al. 2000; Conselice et al. 2001; Edwards et al. 2002; Stein et al. 1997).

At a more fundamental level, kinematic studies of clusters help establish cluster membership independent of and complementary to other methods designed to determine background contamination. Most studies of the cluster galaxy-luminosity function (LF), for example, make use of dedicated control fields to statistically determine the background contribution to the cluster fields. This approach assumes that the control field is representative of the cluster’s background population; the existence of significant cosmic field-to-field variance in deep galaxy counts (Hradecky et al. 2000) partly undermines this assumption and necessarily introduces large uncertainties into the final luminosity function results. Only for the nearest clusters such as Virgo, Fornax, and Centaurus have morphological means been used to determine the membership status of each galaxy (see Jerjen & Dressler (1997)). When morphological information is not available, or to supplement it, some studies make use of surface brightness and color information (Secker et al. 1997) to single out members. None of these methods is entirely satisfactory, especially when they are used in isolation. While the statistical method relies on assumptions and possible systematic biases (which could be present if clusters are initially picked out, for example, due to higher background densities), morphological or color selection methods may miss entire populations of dwarf galaxies such as very compact, M32-like galaxies (Drinkwater & Gregg 1998). Only redshifts can reliably establish cluster membership.

Recent spectroscopic studies illustrate this point. Using kinematic observations to confirm membership of dwarf candidates, Adami et al. (1998) and Secker et al. (1998) have found that Coma contains fewer dwarf members than expected based on the cluster LF determined from statistical subtraction of background counts. Using results from both studies, a combined total of 5 out of 46 galaxies in the magnitude range  $19 < R < 21.3$  were found to be members. Based on the Coma LF measured by Bernstein et al. (1995),  $16 \pm 11$  out of 46 are expected. The quoted error includes the poisson error contribution from both control and cluster counts. Though the count errors in this case are large, this example shows how kinematic observations can test the precision of statistical background galaxy subtraction, especially at the faint end of the LF.

This is particularly relevant in light of recent studies that question the validity of measurements of deep cluster LFs. Valotto et al. (2001) propose that the steep faint-end slopes of LFs which have been found in numerous studies (Driver et al. 1994; de Propris et al. 1995; Trentham 1997a; Smith et al. 1997; Durret et al. 2002) are due to projection effects which cannot be accurately corrected for by subtracting random fields. In a subsequent paper, Val-

otto et al. (2004) argue that Abell clusters, which were initially picked out by eye simply as overdense regions, suffer from background contamination so severe that their cluster status may largely be due to projection effects. One implication is that the faint-end slopes of the LFs of Abell clusters will be systematically overestimated. Supporting evidence comes from clusters detected in X-ray which have LFs that are typically flat, while non X-ray clusters have much steeper faint-end slopes. Since they find no correlation of LF slope with X-ray brightness, they argue that the non X-ray clusters are merely the superposition of multiple poor groups or spurious unbound systems. When background contamination is corrected using random control fields, with presumably fewer background structures, these galaxy counts are undercorrected leaving an excess of galaxies assumed incorrectly to be part of a large cluster population. Since this interpretation questions the accuracy of our census of even local cluster populations, it is important to determine if this is a general problem, and to understand its effects on the galaxy LFs of individual clusters. Kinematic observations are the best way to help address this issue.

The Centaurus Cluster is a nearby ( $z=0.0114$ ) rich and X-ray bright cluster of galaxies. Dickens et al. (1986) were the first to perform a comprehensive study of the Centaurus cluster. They published a catalog of 319 predominantly bright ( $G < 17.5$ ) galaxies including radial velocities for 259 of these. From the redshifts of these bright galaxies, they discovered that the Centaurus cluster exhibits a bimodal velocity distribution. These data suggest that a smaller group centered at 4500 km/s with low velocity dispersion around 260 km/s is infalling into the main body of the cluster, which is centered at around 3000 km/s and has a large velocity dispersion of 933 km/s.

More recently, Jerjen & Dressler (1997) published a deeper catalog of Centaurus galaxies including a substantial dwarf population, using existing du Pont telescope photographic plates covering 2.2 square degrees of the cluster in the B-band. They ascertained cluster membership through morphological criteria. Stein et al. (1997) performed a follow-up spectroscopic study measuring redshifts for 115 galaxies to  $B_T < 19.5$  including 32 new redshifts for dwarf galaxies. Their Centaurus Cluster Catalog (CCC) of likely cluster members was used to select the spectra sample. The majority of these galaxies were found to be members with only a 12% contamination from background galaxies. However, it is unknown what fraction of cluster dwarfs they may have missed when using morphological criteria to establish membership and define the spectroscopic sample.

In this work, we obtain spectra for a random sample of galaxies in the direction of the Centaurus cluster, the only qualification being that they lie within prescribed surface brightness and magnitude ranges. This sample was selected from our photometric observations of the central 0.83 degrees<sup>2</sup> of the Centaurus cluster, the results of which are presented in

Paper I (Chiboucas & Mateo 2006a). This is part of our project to measure the LF faint-end slope in a large sample of nearby clusters in order to establish whether environmental factors impact the shape of the cluster LF and estimate the mass contribution to galaxy clusters by the dwarf population. The aim of this paper is to use kinematics to provide new information with which we can assess the degree of background contamination as faint into the LF as possible.

In section 2 we discuss sample selection and detail the observations. We provide a description of the data reduction in section 3. We present our radial velocity measurements in section 4, with a description of how these are used to determine the galaxy LF of Centaurus in section 5. We conclude with a discussion and summary of our results in section 6. Throughout this work we assume  $H_0 = 70 \text{ km s}^{-1} \text{ Mpc}^{-1}$ .

## 2. Observations

Photometric observations of A3526 (Centaurus,  $z = 0.0114$ ,  $12^h48^m51.8^s -41^\circ18'21''$  2000.0) were acquired with the LCO 1m with a TEK 2K Camera having a field of view of  $20'.48$  and scale size  $0''.6/\text{pixel}$ . The seeing ranged from  $1''.18$  to  $1''.68$  and 2 nights were photometric. Landolt (1992) standard stars were regularly observed on these nights. All data were taken in the V-band for maximum light transmission and the cluster was observed in a mosaic pattern with each field exposed for  $4 \times 15$  minutes for a total exposure of 1 hour. Eleven separate fields were observed to obtain a total coverage of  $0.83 \text{ degrees}^2$ . The photometric sample is complete to  $M_V = -12.4$  and to a surface brightness of  $\sim 25 \text{ mag arcsec}^{-2}$ . The magnitude limit is due primarily to errors in distinguishing between stars and galaxies at fainter magnitudes. Over 10,000 galaxies were detected, but only  $\sim 2700$  to these limits. The reduction process for these data is described in Paper I.

A spectroscopic follow-up was made of  $\sim 500$  of the brightest galaxies in A3526 using the LCO 2.5m with a multi-fiber spectrograph and 2D-Frutti faint object detector. The fibers have a diameter of  $3''.5$  corresponding to a physical size of  $\sim 800 \text{ pc}$  at the distance of the cluster. A  $600 \text{ line mm}^{-1}$  grating was used to obtain a spectral resolution of  $\sim 8.5 \text{ \AA}$  based on FWHM measurements over the region  $3800\text{-}6500\text{\AA}$ . Spectra were taken in 5 different setups with each setup containing 128 fibers including 16 sky fibers. Due to several bad fibers, there were about 106 fibers available in each setup for galaxy spectra acquisition. The spectroscopic sample was chosen to include a random selection of 500 of the brightest galaxies from our Centaurus region galaxy catalog. We did not wish to bias this sample by observing only those galaxies we expected to be cluster members through, for example, morphological criteria. The galaxies within a particular setup all had the same

magnitude and surface brightness range and total exposure times ranged from 2 to 10.6 hours depending on the magnitude limit in each setup. Table 1 provides a summary of the spectroscopic observations. An apparent magnitude of 17 corresponds to  $M_V \sim -16.5$  or to about the bright end of the dwarf population. The magnitudes listed in this table have not been corrected for reddening which is substantial in the direction of Centaurus. Total magnitudes measured hereafter have been corrected to account for  $A_V \sim 0.36$  magnitudes of extinction.

### 3. Processing and Reduction Methods

Photometric data were processed as described in Paper I. The 1D spectra were reduced using the HYDRA package in IRAF. All images were bias corrected and flattened. Individual spectra were extracted using a flat with high S/N to serve as a template where each of the 128 spectra was fit with a 6th order Legendre polynomial. The spectra were then dispersion corrected using arc lamp wavelength calibration spectra taken both before and after each setup exposure. Finally, the spectra were sky subtracted using data from the dedicated 16 sky fibers.

Radial velocities were determined via Fourier cross correlation with a stellar template using the task XCSAO in RVSAO (Kurtz & Mink 1998) on absorption line spectra. Velocity errors (derived from the Tonry & Davis (1979) R values and the width of the cross-correlation peak) typically ranged from 20-120 km/s. Many of the velocities obtained for low surface brightness galaxies, however, were through emission line spectra. These galaxy redshifts were usually identified with O[II] $\lambda$ 3727, Ne[II] $\lambda$ 3869, and the triplet of H $\beta$ , O[III] $\lambda$ 4958.9, and O[III] $\lambda$ 5006.8 and velocities were calculated from an unweighted mean of all emission lines present. We take the standard deviation from these measurements as our error when at least three lines are used. Finally, a heliocentric correction was made for the emission line redshifts. A few examples of the galaxy spectra are shown in Figure 1.

### 4. Radial Velocities

Each of the five setups contain at least 100 spectra and the success rate for determining velocities drops from  $\sim 65\%$  at  $V \leq 17.0$  to  $\sim 20\%$  at  $V \geq 19.0$ . Table 1 lists the number of cluster members and higher redshift galaxies in each setup for which velocities were acquired. A total of 225 radial velocities were obtained to a limiting magnitude of  $V < 19.5$  ( $M_V < -13.9$ ) and with a limiting central surface brightness of  $\mu_o = 23.0$  mag arcsec $^{-2}$ . Radial

velocities for cluster galaxies can be found in Table 2 while those for background galaxies are provided in Table 3. A separate list of those cluster galaxies with new redshifts is given in Table 4. A histogram of all the radial velocities obtained is displayed in Figure 2. In the plot, the Centaurus cluster is obvious at low redshift ( $z = 0.011$ ) while higher redshift structures are apparent at  $cz = 3.8 \times 10^4$  and  $5.6 \times 10^4$  km/s.

Of the galaxies for which velocities were obtained, we found 35% to be member galaxies. We used a cutoff of  $v_{max} = 5450$  km/s for cluster members since this is the  $\sim 3\sigma$  upper limit of the velocity distribution for the higher velocity subcomponent in Centaurus (at 4500 km/s) (Stein et al. 1997). The  $3\sigma$  lower limit is only 200 km/s and is therefore ignored. New redshifts were obtained for 15 Centaurus dwarfs. Of the 78 member galaxies, magnitudes ranged from  $11.8 < V < 18.5$  ( $-21.6 < M_V < -14.9$ ) with central surface brightnesses brighter than 22.5 mag/arcsec<sup>2</sup>. We consider 25 galaxies with  $M_V > -17.0$  to be dwarfs. For some galaxies we have radial velocity measurements from both emission and absorption lines. Comparing the results for 34 galaxies for which both measurements were obtained, we find a mean offset in  $v_{abs} - v_{em}$  of 60.2 km/s, with  $\sigma_{\Delta v} = 198.3$  and  $\sigma_{\overline{\Delta v}} = 34.0$ .

Four cluster galaxies for which we obtained new redshifts are not included in the Centaurus Cluster Catalog of Jerjen & Dressler (1997). These are all compact or compact disk galaxies, which, through morphological means were not classified as cluster members. We display these galaxies in Figure 3, along with a fifth similar compact dwarf. From an all-object spectroscopic survey in Fornax, Drinkwater et al. (2000) have found a new population of ultra compact dwarf galaxies (UCDs) which are often overlooked in typical galaxy surveys. This underscores the importance of using spectra or some other means besides morphology to establish cluster membership.

In Figure 4, we compare our velocities to those in the literature<sup>1</sup>. The majority of velocities for cluster dwarf galaxies come from Stein et al. (1997). We find good agreement with the literature values with a mean difference between our values and the literature of  $-4.3$  km/s with  $\sigma = 97.8$  and  $\sigma_{\overline{\Delta}} = 11.7$ . A comparison of our data to just those of Stein et al. (1997) yields a mean difference of  $-6.2$  km/s with  $\sigma = 105.6$  and  $\sigma_{\overline{\Delta}} = 15.1$ .

In Figure 5 we display the recovery of redshifts as a function of mean isophotal surface brightness. We find that all the highest surface brightness galaxies are cluster members after which the cluster fraction exhibits a sharp drop-off. This is in large part due to the difficulty in obtaining spectra for low surface brightness objects. The fraction of galaxies for which we

---

<sup>1</sup>This research has made use of the NASA/IPAC Extragalactic Database (NED) which is operated by the Jet Propulsion Laboratory, California Institute of Technology, under contract with the National Aeronautics and Space Administration.

obtained spectra but were unable to extract redshifts begins to rise at a surface brightness of  $22.0 \text{ mag arcsec}^{-2}$ , and by  $25.0 \text{ mag arcsec}^{-2}$  we are unable to measure any redshifts. We note that we are able to measure redshifts for more distant galaxies a half magnitude fainter than the cluster members. This may be due to the presence of emission lines in the non-cluster galaxies. Emission lines can be used to determine redshifts even when the galaxy continuum is too low to measure and the spectrum too noisy to use absorption lines. Cluster galaxies tend to have less gas and lower star formation rates, particularly those galaxies near the cluster core, and are therefore less likely to have emission line spectra (Giovanelli et al. 1982; Biviano et al. 1997). Thus, we also distinguish in Figure 5 between the fractions recovered with and without emission lines. We find that in the faintest surface brightness bin where we obtain redshifts for distant galaxies only, all velocities are obtained through emission lines.

## 5. Luminosity Function

We can use our kinematic results to help improve on our estimate of background contamination in our photometric determination of the Centaurus LF. We first determined the fraction of members to the total number of galaxies for which redshifts were obtained in each half magnitude bin. Using these fractions, along with the binned number of galaxies per square degree detected in the cluster fields, we calculated the expected number of members in each half magnitude bin. In Figure 6 we show the LF constructed using the redshift determined member fractions along with the LF derived from the background subtraction method using nearby control fields described in Paper III (Chiboucas & Mateo 2006b). At magnitudes brighter than  $M_V < -18.4$ , neither the control fields nor the spectra turned up any background galaxies. These points are therefore identical. Member counts from redshifts only extend to  $M_V = -15.0$ . The cluster galaxy counts obtained in this way fall below counts calculated statistically. This is likely because our calculated fraction of member dwarf galaxies to background galaxies is too small due to either the lower surface brightness of the dwarfs, or because the background galaxies more often have emission lines and are preferentially recovered.

In Figure 7, we plot the fraction of member and non-member galaxies in each magnitude bin with radial velocities that were measured with emission line spectra. In the faintest magnitude bins, where only high redshift galaxies are recovered, 40 - 50% of these had emission lines. This, of course, means that at least half were recovered through absorption line spectra and it is therefore possible to measure redshifts at these magnitudes without the presence of emission lines. It also shows a lack of emission line spectra in dwarf galaxies at

these magnitudes.

It is likely that we are unable to extract velocities from the spectra for a large population of low surface brightness non-emission line cluster members. We plot the central surface brightness vs. total magnitude for all galaxies for which we obtained spectra in Figure 8. The central surface brightnesses were determined from surface brightness profile fitting as described in Paper I and are uncorrected for seeing effects. We can define a region in this  $\mu_o - V$  space which encloses most member galaxies. It is apparent from this plot that most dwarf galaxies have much lower surface brightnesses than background galaxies at a given magnitude. This could account for the fewer cluster galaxies recovered by the spectra than would be expected from the LF counts determined using statistical background correction methods.

We therefore use these surface brightness regions to make a correction for the large number of galaxies for which we were unable to extract redshifts. Central surface brightnesses and magnitudes for galaxies for which we obtained spectra but were unable to measure redshifts are plotted in Figure 9. For simplicity, we assume that all galaxies lying within the region denoted as ‘Background’ are background galaxies and the rest are cluster members. While there will be some cross-contamination, it does not appear to be severe and, if anything, will overestimate the number of cluster members. After including these counts as members or background galaxies, we again determine the fraction of cluster members in each magnitude bin and use these to calculate the total number of cluster members from the total observed counts in each magnitude bin. The LF is shown in Figure 10.

We find that counts are now only slightly lower than those calculated statistically. A  $\mu_o - V$  plot of all galaxies found in the Centaurus fields (Figure 11) reveals that there is still a population of galaxies with even lower surface brightness beyond those for which we tried to obtain spectra. We should therefore still be underestimating the dwarf population.

As one final estimate of the LF, we use the  $\mu_o - V$  regions to define the membership status for each galaxy from our complete catalog of Centaurus galaxies (see Paper I). In order to do so, we must extrapolate the surface brightness selection line by about 2.5 magnitudes to reach our photometric survey limits. At fainter magnitudes and surface brightnesses, errors are larger so we expect the contamination to increase as larger errors cause points to migrate relative to the selection line. In Figure 12, we display the luminosity function for galaxies determined in this manner to be cluster members. Counts are now slightly higher than those calculated through statistical means, but only around the  $1\sigma$  level. Differences are expected because the two LFs are constructed in different ways. The original LF counts are weighted averages which include corrections for completeness and misclassification whereas here we use the complete catalog to directly determine membership. It is also likely that we are

overestimating the member fraction as the contamination from background galaxies in the low surface brightness region appears to be slightly greater than of cluster galaxies in the high surface brightness region (see Figure 8). A best fit using a Schechter function (Schechter 1976) for the statistical LF yields a faint-end slope,  $\alpha$ , of  $-1.42$  and  $M_V^*$  of  $-21.25$  while a power law fit to just the faint-end finds a best fit slope of  $-1.40$ . For a complete description of the measurement of this LF, see Paper III. The slope of the LF using surface brightness criteria does not differ significantly from the statistical LF. While the normalization is slightly higher, this LF is best fit with a Schechter function having  $\alpha = -1.40$  and  $M_* = -21.22$ . The statistically determined LF exhibits a drop-off in counts in the magnitude range  $-15 < M_V < -12$  followed by a steepening at the faintest magnitudes which is not mimicked by the LF established with surface brightness criteria. Rather, this LF maintains a constant slope until a turnover due to incompleteness at  $M_V = -12$ .

This surface brightness criteria LF we have constructed is presumed to be an overestimate of member galaxies since we have drawn the division lines to include as many members as possible. However, it is possible, given the few data points in Figure 8 which we use to establish the membership criteria, to use other delineations which are still consistent with the data. To determine the systematic uncertainty in the faint-end slope using this method, we redraw the division lines in Figure 8 such that they minimize and maximize the number of galaxies labelled as background while remaining consistent with the spectroscopy results. When measuring the lower limit of the faint-end slope, we also push the bright-end division line to fainter magnitudes, consistent with the data. This produces a lower (shallower) value for the faint-end slope of  $\alpha = -1.22$ . We find an upper limit to the slope of  $-1.50$ . Random errors such as magnitude or surface brightness measurement errors will increase this uncertainty.

## 6. Discussion

We have used spectroscopic redshifts of 225 galaxies to assist in constructing the Centaurus cluster galaxy LF and compare to our photometric LF obtained with a statistical background correction using nearby control fields. We find counts and slope lower when strictly using the spectroscopic results than from the statistically corrected photometric sample. However, it is clear that distant late type emission line and higher surface brightness galaxies are easier to obtain spectra for than low surface brightness (LSB) cluster dwarfs at the same faint magnitudes. When we make use of the separation between distant and member galaxies on a magnitude - surface brightness plane, we find a similar faint-end slope compared to the control field subtracted LFs ( $-1.40$  vs  $-1.42 \pm 0.2$ ) although the faint-end

slope for the  $\mu_o - V$  division case could realistically range from  $-1.22$  to  $-1.50$ . Errors using either method are similar and both may suffer from similar systematics (see below).

First we explore the cause of the  $\mu_o - V$  division between background and cluster galaxies. Background galaxies appear to primarily lie in a clump within a small range of surface brightness and magnitude (between  $19 < \mu_o < 22$  and between  $16.5 < V < 20$ ). If we take a bright elliptical galaxy in Centaurus with a  $V$  magnitude of 13.4 ( $M_V = -20$ ), central surface brightness of  $13.9 \text{ mag/arcsec}^2$ , and half-light radius,  $R_e$ , of  $12''.2$  and shift it to a redshift of 0.1 (about the distance of the first large background structure), we find that  $R_e$  reduces to  $1''.5$ , which is approximately the average seeing for our survey. According to Trujillo et al. (2001), even in the case of our best seeing image,  $1''.1$ , Sersic profile fitting should recover  $R_{e(rec)} \sim 3.5 R_{e(true)}$  and  $I_{o(rec)} \sim 0.0015 I_{o(true)}$  when this seeing is not taken into account. The central surface brightness for this galaxy would accordingly be inflated to  $20.9 \text{ mag/arcsec}^2$  with  $V = 18.3$ , within the range of the background clump. Thus, the separation between background and cluster galaxies in our surface brightness – magnitude plots is an artifact of seeing where the cluster members are primarily those galaxies which are resolved. Using this surface brightness – magnitude criteria for membership we do not expect to exclude many dwarf galaxies unless there is a large population of very compact dwarfs, nor do we expect a large population of giant resolved background galaxies to contaminate the cluster member region.

While the method of using redshifts to establish cluster membership should be more accurate than the statistical method for estimating the background contribution, we find that it does have shortcomings. First, there is a selection bias in that galaxies for which spectra are taken must be chosen ahead of time. Since even multi-fiber spectrographs have a limit to the number of spectra which can be obtained for each exposure and exposures for faint, low surface brightness galaxies must be long, often there is a selection bias for choosing galaxies which are likely to be cluster members. Although we randomly chose our sample based entirely on magnitude and surface brightness ranges, Stein et al. (1997), for example, select their spectroscopic sample from their Centaurus Cluster Catalog which contains galaxies likely to be Centaurus cluster members based on morphological criteria. As we have found, some compact cluster members may be missed in this way. Furthermore, low surface brightness and highly compact galaxies must first be cataloged in photometric studies and it is possible that an entire population of low surface brightness dwarf galaxies may be missed.

Second, and more importantly, spectra can only be obtained for brighter, high surface brightness galaxies or for galaxies with emission lines (unless much larger telescopes are used). Spectroscopic studies finding fewer galaxies than might be expected at fainter magnitudes

are likely simply unable to obtain measurable spectra for large numbers of dEs with low surface brightnesses and low star formation rates. Our spectra yield redshifts at the faintest surface brightnesses for emission line background galaxies only. We find that we are unable to extract velocities from spectra for a large fraction of low surface brightness galaxies in each magnitude bin which are likely, based on our spectra results, to be preferentially member galaxies. Thus, any spectroscopic study of nearby cluster galaxies will be systematically biased toward recovering redshifts for background galaxies.

A further important consideration is the depth of the study. De Propris et al. (2003) measure a faint-end slope for cluster galaxies of  $-1.28 \pm 0.03$  from the 2dF galaxy redshift survey down to a limiting magnitude of  $M_{b,j} < -15$ . While they do not find a steep slope, they also have a fairly bright limiting magnitude, similar to this work. Many photometric studies which find steep slopes probe to much fainter limiting magnitudes (eg. Trentham (1997b, 1998); Phillipps et al. (1998); de Propris et al. (1995)). If a steeper upturn does exist at faint magnitudes, it would be difficult to observe with spectroscopic studies which do not reach these fainter magnitudes.

While there are limitations to using spectra to establish membership, constructing the LF through statistical means faces great uncertainties due to field-to-field variance. This method assumes that background galaxy counts are similar in both cluster and control fields. However, it is known that counts can vary from field to field by as much as 19–50% on scales of  $0^\circ.4 - 0^\circ.5$  degrees (Hradecky et al. (2000) and references therein). In addition, clusters which are originally discovered by eye may be biased towards regions of greater density contrast with their surroundings. Valotto et al. (2004) argue that Abell clusters may have been picked out due to projection effects and suffer from severe background contamination. While the spectra results presented here for Centaurus, Abell 3526, corroborate the LF slope measured statistically, this is an X-ray bright cluster. It may be worth using a similar technique on other nearby, non X-ray clusters to determine whether statistically corrected LF faint-end slopes of these clusters are systematically inflated.

The LF has been studied in numerous nearby clusters using various means to distinguish between members and nonmembers. These studies have turned up a wide range of values for the faint-end slope spanning  $-2.3 < \alpha < -1.3$  (see e.g. Trentham (1997b); Trentham et al. (2001); de Propris et al. (1995); Valotto et al. (1997) and Bernstein et al. (1995)). Whether this implies intrinsic differences exist between galaxy formation and/or evolutionary histories in these clusters or whether the differences are simply due to the different methods used to construct the galaxy LF and in dealing with the selection effects inherent in detecting low surface brightness dwarf galaxies remains an unanswered question. We find no evidence of a very steep slope from either method employed here. While it is possible that we could be

missing a large population of LSB dwarf galaxies, we do not believe this to be the case as we discuss in greater detail in paper III.

To address the question of whether the cluster LF faint-end varies or has a universal slope, it is critical to establish the faint-end slope in a number of clusters. Correcting for background contamination statistically using nearby control fields where counts are expected to vary from the true cluster background is fraught with large uncertainties. To accurately construct a cluster LF, membership must be determined to faint limiting magnitudes directly. For higher redshift clusters, it may be possible to use photometric redshifts to establish membership (see ie. Toft et al. (2004)). For the nearest clusters, namely Virgo, Fornax, and Centaurus, some researchers have chosen to establish membership based on morphology. We find that some compact galaxies may be missed in this way, although only at around the 3-6% level. While UCDs are known to exist in clusters (Drinkwater et al. 2000), these galaxies have magnitudes of around  $M_V = -12.0$ , typically at or below the magnitude limit of most surveys. Stein et al. (1997) found only a 12% contamination rate of background galaxies in their morphologically determined cluster sample using follow-up spectroscopy, so membership determined in this manner is likely to be more reliable than through statistical approximation. For other nearby clusters, other methods for measuring distances to the dwarf galaxies and establishing cluster membership need to be devised, or spectra must be acquired to fainter limiting magnitudes and much lower surface brightnesses with more sensitive instruments and larger telescopes to firmly establish the faint-end slope in at least a few clusters. While it is very difficult to obtain spectra to the necessary surface brightnesses, we demonstrate that it may be possible to use spectra in conjunction with other properties to obtain better estimates of the nearby galaxy cluster LF.

We thank the anonymous referee for very helpful suggestions which have improved the analysis and presentation of this paper. KC would like to thank Joe Mohr for providing the stellar template for extracting radial velocities from absorption line spectra.

## REFERENCES

- Adami, C., Nichol, R. C., Mazure, A., Durret, F., Holden, B., & Lobo, C. 1998, *A&A*, 334, 765
- Aguero, E. L., Suarez, F., & Paolantonio, S. 1995, *PASP*, 107, 959
- Bernardi, M., Alonso, M. V., da Costa, L. N., Willmer, C. N. A., Wegner, G., Pellegrini, P. S., Rit e, C., & Maia, M. A. G. 2002, *AJ*, 123, 2990

- Bernstein, G. M., Nichol, R. C., Tyson, J. A., Ulmer, M. P., & Wittman, D. 1995, *AJ*, 110, 1507+
- Bertin, E. & Arnouts, S. 1996, *A&AS*, 117, 393
- Biviano, A., Katgert, P., Mazure, A., Moles, M., den Hartog, R., Perea, J., & Focardi, P. 1997, *A&A*, 321, 84
- Chiboucas, K. & Mateo, M. 2006a, in preparation
- . 2006b, in preparation
- Conselice, C. J., Gallagher, J. S., & Wyse, R. F. G. 2001, *ApJ*, 559, 791
- De Propris, R., Colless, M., Driver, S. P., Couch, W., Peacock, J. A., Baldry, I. K., Baugh, C. M., Bland-Hawthorn, J., Bridges, T., Cannon, R., Cole, S., Collins, C., Cross, N., Dalton, G. B., Efstathiou, G., Ellis, R. S., Frenk, C. S., Glazebrook, K., Hawkins, E., Jackson, C., Lahav, O., Lewis, I., Lumsden, S., Maddox, S., Madgwick, D. S., Norberg, P., Percival, W., Peterson, B., Sutherland, W., & Taylor, K. 2003, *MNRAS*, 342, 725
- de Propris, R., Pritchet, C. J., Harris, W. E., & McClure, R. D. 1995, *ApJ*, 450, 534+
- de Vaucouleurs, G., de Vaucouleurs, A., Corwin, H. G., Buta, R. J., Paturel, G., & Fouque, P. 1991, *Third Reference Catalogue of Bright Galaxies (Volume 1-3, XII, 2069 pp. 7 figs.. Springer-Verlag Berlin Heidelberg New York)*
- Dickens, R. J., Currie, M. J., & Lucey, J. R. 1986, *MNRAS*, 220, 679
- Drinkwater, M. J. & Gregg, M. D. 1998, *MNRAS*, 296, L15+
- Drinkwater, M. J., Jones, J. B., Gregg, M. D., & Phillipps, S. 2000, *Publications of the Astronomical Society of Australia*, 17, 227
- Driver, S. P., Phillipps, S., Davies, J. I., Morgan, I., & Disney, M. J. 1994, *MNRAS*, 268, 393+
- Durret, F., Adami, C., & Lobo, C. 2002, *A&A*, 393, 439
- Edwards, S. A., Colless, M., Bridges, T. J., Carter, D., Mobasher, B., & Poggianti, B. M. 2002, *ApJ*, 567, 178
- Gavazzi, G., Zaccardo, A., Sanvito, G., Boselli, A., & Bonfanti, C. 2004, *A&A*, 417, 499

- Geha, M., Guhathakurta, P., & van der Marel, R. P. 2003, *AJ*, 126, 1794
- Giovanelli, R., Haynes, M. P., & Chincarini, G. L. 1982, *ApJ*, 262, 442
- Hradecky, V., Jones, C., Donnelly, R. H., Djorgovski, S. G., Gal, R. R., & Odewahn, S. C. 2000, *ApJ*, 543, 521
- Jerjen, H. & Dressler, A. 1997, *A&AS*, 124, 1
- Kurtz, M. J. & Mink, D. J. 1998, *PASP*, 110, 934
- Landolt, A. U. 1992, *AJ*, 104, 340
- Lauberts, A. & Valentijn, E. A. 1989, *The surface photometry catalogue of the ESO-Uppsala galaxies (Garching: European Southern Observatory, —c1989)*
- Mathewson, D. S. & Ford, V. L. 1996, *ApJS*, 107, 97
- Pedraz, S., Gorgas, J., Cardiel, N., Sánchez-Blázquez, P., & Guzmán, R. 2002, *MNRAS*, 332, L59
- Phillipps, S., Parker, Q. A., Schwartzberg, J. M., & Jones, J. B. 1998, *ApJ*, 493, L59
- Schechter, P. 1976, *ApJ*, 203, 297
- Secker, J., Harris, W. E., Côté, P., & Oke, J. B. 1998, in *Untangling Coma Berenices: A New Vision of an Old Cluster*, 115–+
- Secker, J., Harris, W. E., & Plummer, J. D. 1997, *PASP*, 109, 1377
- Smith, R. J., Lucey, J. R., Hudson, M. J., Schlegel, D. J., & Davies, R. L. 2000, *MNRAS*, 313, 469
- Smith, R. M., Driver, S. P., & Phillipps, S. 1997, *MNRAS*, 287, 415
- Stein, P. 1996, *A&AS*, 116, 203
- Stein, P., Jerjen, H., & Federspiel, M. 1997, *A&A*, 327, 952
- Toft, S., Mainieri, V., Rosati, P., Lidman, C., Demarco, R., Nonino, M., & Stanford, S. A. 2004, *A&A*, 422, 29
- Tonry, J. & Davis, M. 1979, *AJ*, 84, 1511
- Trentham, N. 1997a, *MNRAS*, 290, 334

—. 1997b, MNRAS, 286, 133

—. 1998, MNRAS, 293, 71

Trentham, N., Tully, R. B., & Verheijen, M. A. W. 2001, MNRAS, 325, 385

Trujillo, I., Aguerri, J. A. L., Cepa, J., & Gutiérrez, C. M. 2001, MNRAS, 328, 977

Valotto, C. A., Moore, B., & Lambas, D. G. 2001, ApJ, 546, 157

Valotto, C. A., Muriel, H., Moore, B., & Lambas, D. G. 2004, ApJ, 603, 67

Valotto, C. A., Nicotra, M. A., Muriel, H., & Lambas, D. G. 1997, ApJ, 479, 90+

van Zee, L., Skillman, E. D., & Haynes, M. P. 2004, AJ, 128, 121

Table 1. Spectroscopic Observations

Setup	Exposure Time (hr)	V range	$\mu_o$ (mag/arcsec <sup>2</sup> )	# Cluster members	# Higher redshift
100	2	12-17	20-23	57	8
300	7	17-18	21-23	15	49
500	6	18-19	21-24	2	39
700	9	18-19	22-23	3	31
900	10.6	19+	23-24	2	20
Totals				78	147

Table 2. Cluster Members

$\alpha$ 2000.0	$\delta$	$V$ total <sup>a</sup>	$v_{rad}$ Absorption	Error	$v_{rad}$ Emission	Error	$v_{rad}$ Literature	Error	reference <sup>b</sup>
12 47 30.15	-41 39 02.60	16.23	3743	73			3527	59	1
12 47 33.42	-41 07 54.70	15.94	3647	130	3740	160	3848	50	1
12 47 45.05	-41 09 21.30	16.52	2689	76			2750	43	1
12 47 49.22	-40 59 54.90	15.85	3186	58			3026	29	1
12 47 52.20	-41 20 13.60	18.05	2828	88					
12 47 54.18	-41 03 44.90	15.56	4464	60					
12 47 55.84	-40 54 16.50	17.33	1817	74					
12 47 56.01	-40 55 14.00	14.52	3862	63			3874	70	1
12 47 58.97	-41 11 21.30	15.25	3117	50			3088	50	1
12 47 59.57	-41 13 11.40	14.78	4048	43			4063	19	1
12 48 02.02	-41 18 19.10	16.73	2473	101			2329	33	1
12 48 07.29	-41 37 46.30	18.34	4188	106					
12 48 15.45	-41 42 57.20	16.97	3855	83			3925	45	1
12 48 15.82	-41 18 57.70	17.84			4256	28	4278	58	1
12 48 16.68	-41 26 10.60	17.34	2118	90					
12 48 22.75	-41 07 23.50	13.90	3657	27			3641	49	4
12 48 30.72	-41 01 18.10	14.95	4231	31			4069		1
12 48 31.00	-41 18 23.60	15.13	2971	32			2973	44	1
12 48 36.06	-41 26 23.40	16.85	3346	83			3304	60	1
12 48 39.69	-41 16 05.60	16.32	2659	95			2910	67	1
12 48 43.43	-41 38 37.40	14.05	2240	30			2193	19	1
12 48 48.56	-41 20 53.50	17.78	3053	40					
12 49 02.00	-41 15 33.30	17.39	2075	70			1958	71	1
12 49 03.16	-41 23 29.50	15.49	5227	52			5298	28	1
12 49 04.12	-41 20 19.60	14.51	3714	185			3469	34	3
12 49 09.63	-41 11 33.90	16.43	3192	64			3122	29	1
12 49 12.04	-41 32 40.80	14.33	2809	33			2838	20	6
12 49 18.59	-41 20 07.80	15.28	3093	33			3108	19	1
12 49 22.68	-41 15 18.60	18.17	3620	108			3652	61	1
12 49 25.43	-41 25 45.80	15.67	4048	58			4076	29	1
12 49 26.21	-41 29 20.80	13.37	4230	22			4271	21	4
12 49 26.69	-41 27 46.50	13.43	4866	113			4831		6
12 49 30.20	-41 25 15.70	17.63	2827	61			2818	30	1
12 49 37.85	-41 23 17.70	13.72	3628	24			3627	24	4
12 49 40.14	-41 21 58.30	16.01	3107	131			2880	40	1
12 49 41.96	-41 13 45.50	16.17	3657	69			3715	26	1
12 49 51.56	-41 13 34.70	13.69	2202	30			2160	23	1
12 49 54.18	-41 16 45.50	13.50	3822	25			3862	4	5
12 49 56.00	-41 24 04.40	17.33	4640	83			4661	69	1
12 50 03.88	-41 22 55.10	11.32	4614	28			4678	4	5
12 50 11.53	-41 13 15.80	14.12	2928	25			2908	26	1
12 50 11.86	-41 17 56.90	15.45	4105	49			4172	33	8
12 50 12.15	-41 30 56.00	13.00	2458	29			2384	24	1
12 50 22.00	-41 23 37.00	16.85	4450	77					
12 50 33.51	-41 20 09.80	16.31	2278	95					

Table 2—Continued

$\alpha$ 2000.0	$\delta$	$V$ total <sup>a</sup>	$v_{rad}$ Absorption	Error	$v_{rad}$ Emission	Error	$v_{rad}$ Literature	Error	reference <sup>b</sup>
12 50 34.37	-41 28 15.10	13.38	5316	31			5302	6	5
12 50 34.63	-41 27 07.10	17.30	4608	128					
12 50 57.45	-41 23 47.60	14.34	4450	37			4445	19	1
12 50 58.90	-41 29 40.20	17.39	2112	87			2139	36	1
12 51 00.86	-41 43 21.10	13.37	2521	34			2469	23	1
12 51 08.89	-41 40 12.30	16.25	2646	85					
12 51 32.84	-41 13 39.90	13.99	4775	35			4771	24	1
12 51 36.34	-41 29 32.50	15.13	3669	70			3864	23	1
12 51 37.31	-41 18 12.80	13.91	3502	33			3445	22	1
12 51 39.78	-41 28 55.60	17.14	5021	23			4879	58	1
12 51 47.95	-40 59 37.50	14.68	2657	29			2722	47	1
12 51 50.83	-41 11 10.60	15.23	4736	37			4712	18	1
12 51 51.30	-41 25 56.50	16.41	3560	60			3624	22	1
12 51 56.43	-41 32 20.70	13.86	3695	29			3682	19	1
12 52 02.09	-41 25 07.60	16.97	3075	64			3329	76	1
12 52 02.38	-41 21 11.70	17.06	4327	68					
12 52 03.08	-41 27 34.60	13.89	4000	22			3945	3	5
12 52 12.97	-41 20 20.40	14.34	5134	80			5107	31	1
12 52 15.47	-41 28 37.20	15.49	3119	72			3037	26	1
12 52 15.69	-41 15 33.60	14.62	3476	52			3388	23	1
12 52 16.02	-41 23 26.80	13.31	3015	20			2984	23	4
12 52 19.55	-41 03 36.60	12.34	3381	36			3389	26	1
12 52 21.52	-41 10 00.60	17.24			4881	23	4881	45	1
12 52 22.61	-41 16 55.81	13.94	4627	27			4611		1
12 52 30.41	-40 55 43.10	15.69			2853	37			
12 52 32.86	-41 09 44.00	17.81			4553	44			
12 52 34.82	-41 13 33.60	17.40	4801	39			4971	71	1
12 52 35.13	-41 17 23.80	18.11			5059	113			
12 52 40.91	-41 13 47.20	14.71	4764	41			4858	23	1
12 52 42.58	-41 09 57.70	15.66	4333	36					
12 52 50.18	-41 20 14.70	12.92	4798	27			4868	45	7
12 53 14.03	-41 08 27.50	16.45	2845	114			2766	43	1
12 53 20.19	-41 38 07.50	13.61	4829	32	4840	50	4796	25	9

<sup>a</sup>Total magnitudes from SExtractor(Bertin & Arnouts 1996)

<sup>b</sup>references: (1)Stein et al. (1997) (2)Dickens et al. (1986) (3)Mathewson & Ford (1996) (4)Stein (1996) (5)Smith et al. (2000) (6)Lauberts & Valentijn (1989) (7)de Vaucouleurs et al. (1991) (8)Bernardi et al. (2002) (9)Agüero et al. (1995)

Table 3. Background Galaxies

$\alpha$ 2000.0	$\delta$	$V$ total <sup>a</sup>	$v_{rad}$ Absorption	Error	$v_{rad}$ Emission	Error	$v_{rad}$ Literature	Error	reference <sup>b</sup>
11 47 28.96	-41 17 02.10	18.60	11485	204					
12 47 35.07	-41 10 46.90	19.51	55887	72					
12 47 36.50	-41 21 36.20	18.15	38448	65	38510				
12 47 39.15	-41 22 08.60	19.19	38723	131	38416	92			
12 47 41.18	-41 13 24.30	18.78	63146	54	63291	85			
12 47 43.60	-41 10 10.90	16.11	55845	63	55891				
12 47 47.34	-41 36 07.70	17.63			31845	81			
12 47 47.44	-41 37 28.70	19.55	70386	104					
12 47 48.39	-41 22 38.40	17.92	38400	89	38453				
12 47 50.02	-41 16 33.70	18.89	45664	94	46003				
12 47 52.07	-41 12 01.50	19.18	70459	107					
12 47 54.18	-41 38 59.00	17.50	25994	67					
12 47 55.98	-41 00 24.70	19.43	29069	64					
12 47 59.11	-41 25 30.10	18.15	40275	75					
12 48 01.58	-41 26 52.80	18.43	70446	111	70356				
12 48 01.86	-40 54 41.20	18.54	55424	73					
12 48 05.72	-41 36 35.70	19.36	71829	97					
12 48 09.69	-41 12 20.60	18.08	55980	57					
12 48 14.83	-41 23 35.90	19.40	70420	140	70160				
12 48 15.63	-40 59 40.50	19.00	45771	114	45945	37			
12 48 17.54	-40 59 49.70	18.41	55607	84					
12 48 18.88	-41 38 22.70	18.32	45831	83					
12 48 19.57	-40 58 50.30	18.87	56054	113					
12 48 22.31	-41 11 33.30	18.88	26129	76	25902	18			
12 48 24.25	-41 13 16.80	19.17	55296	113					
12 48 25.34	-41 26 07.00	18.75	56146	84	55913				
12 48 27.94	-41 09 02.70	17.23	33594	102			33639	69	4
12 48 28.17	-41 21 46.00	18.35	49722	148	46740				
12 48 28.62	-40 59 07.00	18.83	51793	106	51755				
12 48 29.19	-41 27 21.20	17.88	46633	78					
12 48 32.84	-41 15 35.00	18.28	38544	115	38509				
12 48 36.46	-41 32 30.00	19.35	55295	89					
12 48 37.36	-41 19 15.30	18.07	33146	86	33121	48			
12 48 37.98	-41 27 10.20	18.04	39754	83	39720				
12 48 38.41	-41 20 28.90	18.52	22032	107	25631				
12 48 38.77	-41 07 05.50	17.56	38504	83					
12 48 39.71	-41 12 13.10	18.40	56277	142					
12 48 40.49	-41 28 32.70	18.95	46565	144	46766				
12 48 42.12	-41 26 50.90	18.47	46457	99	46554				
12 48 43.51	-41 28 21.00	19.75	72840	106	72243				
12 48 43.95	-41 34 03.10	18.57	32933	88					
12 48 46.81	-41 43 35.40	18.44			60896	55			
12 48 47.25	-41 33 21.60	19.23	55105	108	55136				
12 48 48.57	-41 16 16.60	17.35	56008	83					
12 48 52.40	-41 44 50.20	18.49	69847	89					

Table 3—Continued

$\alpha$ 2000.0	$\delta$	$V$ total <sup>a</sup>	$v_{rad}$ Absorption	Error	$v_{rad}$ Emission	Error	$v_{rad}$ Literature	Error	reference <sup>b</sup>
12 48 54.22	-41 30 12.20	18.03	39735	103	39739	266			
12 48 54.93	-41 39 31.00	18.73	15900	118					
12 48 56.80	-41 15 33.60	19.23	55885	70					
12 48 57.78	-41 26 49.80	18.10	56103	80					
12 49 00.39	-41 32 55.90	18.68	29027	107	29035				
12 49 00.88	-41 25 42.20	17.76	16626	81			16514	64	1
12 49 02.82	-40 59 41.70	17.96	14769	35					
12 49 05.27	-41 10 50.50	18.31	60715	66					
12 49 05.36	-41 24 09.00	17.61	55683	62					
12 49 06.22	-41 17 51.20	16.65	56099	83					
12 49 07.27	-41 31 07.50	18.24	47355	56					
12 49 09.02	-41 41 15.90	17.54	39564	80					
12 49 09.67	-41 35 35.80	17.57	39596	73					
12 49 15.05	-41 18 37.60	17.46	26286	45					
12 49 17.15	-41 35 50.80	19.25	56310	97					
12 49 19.78	-41 15 59.20	18.40	34244	130	34001				
12 49 20.53	-41 38 46.50	19.02			14454	51			
12 49 20.70	-41 19 17.02	17.39	25394	61					
12 49 24.37	-41 36 59.90	19.00	56048	77					
12 49 25.59	-41 30 24.90	17.09			10676	40			
12 49 28.66	-41 34 31.60	18.54	71243	72					
12 49 30.27	-41 22 34.90	19.43	55934	84					
12 49 30.39	-41 18 18.00	19.21			55016	116			
12 49 31.39	-41 13 40.20	18.51			9381	73			
12 49 36.56	-41 16 41.90	18.99	12642	180					
12 49 41.54	-41 41 50.40	19.18			22259	74			
12 49 48.99	-41 39 38.90	19.69	64656	97					
12 49 51.91	-41 13 58.30	18.36	13238	102					
12 49 59.16	-41 36 16.40	17.95	71651	91					
12 50 00.85	-41 43 26.50	16.79	16321	88			16362	45	1
12 50 07.93	-41 26 27.80	18.46	55911	68					
12 50 11.35	-41 10 05.00	19.40	27181	102					
12 50 12.02	-41 28 25.80	16.59	16234	53					
12 50 14.76	-40 58 14.20	19.29	69788	93					
12 50 14.95	-41 04 04.70	19.43	82514	80					
12 50 17.73	-41 23 55.50	18.93	47318	84					
12 50 20.17	-41 38 16.30	18.52	26698	110					
12 50 21.84	-40 55 42.70	19.35	25980	90	25941	44			
12 50 27.31	-41 26 00.20	17.65	44786	120	44650				
12 50 40.32	-40 55 46.20	16.79	28935	64					
12 50 43.02	-41 24 39.10	18.48	56375	87					
12 50 45.94	-40 57 40.80	19.39	61826	93					
12 50 46.24	-41 07 23.50	17.66	33438	166	33204				
12 50 55.08	-40 58 11.40	18.46			76101	132			
12 50 55.72	-41 21 46.90	18.58			56028	104			

Table 3—Continued

$\alpha$ 2000.0	$\delta$	$V$ total <sup>a</sup>	$v_{rad}$ Absorption	Error	$v_{rad}$ Emission	Error	$v_{rad}$ Literature	Error	reference <sup>b</sup>
12 50 57.69	-41 02 06.60	18.39	56562	79	56760				
12 50 57.89	-41 44 42.40	16.51	27458	68					
12 50 58.60	-41 35 10.20	15.38	16376	61			16475		2
12 51 02.78	-41 26 47.50	18.45			10153	84			
12 51 03.57	-41 08 01.40	18.42			13594	53			
12 51 07.60	-41 26 03.90	18.20	56167	129					
12 51 07.80	-41 19 46.10	19.10	46798	99	46334	605			
12 51 09.32	-41 19 12.70	15.31			10653	33	10619		4
12 51 12.55	-41 10 57.80	18.34			10444	52			
12 51 15.57	-41 34 25.60	17.93	21338	100					
12 51 17.72	-41 16 34.10	17.69			10678	59	10679	38	1
12 51 22.97	-40 58 35.40	17.72	30732	72					
12 51 25.87	-41 16 17.80	17.96	42571	103					
12 51 28.39	-41 24 14.00	18.26	72641	118					
12 51 30.71	-41 07 33.80	17.33			8726	52			
12 51 32.52	-41 08 20.40	19.39	8620	148					
12 51 34.51	-41 01 32.40	15.91	33970	49					
12 51 36.05	-41 33 09.10	17.94	7578	73					
12 51 40.04	-41 01 22.90	15.21			25588	75			
12 51 53.29	-40 59 04.70	19.54	70608	96					
12 52 00.55	-41 00 42.90	19.20	56396	106	56567				
12 52 04.10	-41 30 01.00	17.79	27809	79					
12 52 05.03	-41 37 39.80	18.74	19900	160	19706	21			
12 52 05.41	-41 38 39.50	17.02			19413	70	19439	50	1
12 52 05.41	-41 33 48.50	17.26	27947	52					
12 52 06.09	-41 22 27.30	18.14	67457	79					
12 52 06.31	-41 37 35.40	17.58	19546	93					
12 52 08.02	-41 17 57.50	18.52	45370	102					
12 52 13.53	-41 40 50.40	18.80	27296	81					
12 52 19.57	-40 57 06.90	18.70	70087	119					
12 52 23.66	-41 21 28.90	16.89	25030	63			25120		4
12 52 25.49	-41 34 46.80	19.58	29541	70	29413				
12 52 25.91	-41 29 18.10	19.12	6030	132					
12 52 27.34	-41 03 36.60	18.62	56873	116					
12 52 28.73	-41 26 05.40	16.00	31502	67					
12 52 32.22	-41 36 06.30	17.61	27221	76					
12 52 32.86	-41 32 19.50	16.95			29292	80			
12 52 33.30	-41 11 05.20	18.60			44742	50			
12 52 36.05	-41 15 33.90	17.61	23485	53			23457		4
12 52 38.69	-41 30 10.50	17.53	19121	129					
12 52 39.18	-41 23 09.80	17.40	31479	57			31348	45	4
12 52 41.13	-41 15 13.60	17.37	56331	89					
12 52 41.56	-40 58 24.40	17.98	56584	72					
12 52 43.50	-41 18 43.40	18.13	25022	74					
12 52 45.32	-41 28 00.20	16.40	24854	66					

Table 3—Continued

$\alpha$ 2000.0	$\delta$	$V$ total <sup>a</sup>	$v_{rad}$ Absorption	Error	$v_{rad}$ Emission	Error	$v_{rad}$ Literature	Error	reference <sup>b</sup>
12 52 46.99	-41 19 36.30	17.01	56786	79					
12 52 50.67	-41 00 46.00	18.66	37918	116	37717				
12 52 53.10	-41 01 09.40	18.53			14629	109			
12 52 53.45	-41 29 33.60	18.25	9331	63	9136	62			
12 52 55.06	-41 12 28.60	18.67			19566	35			
12 52 57.21	-41 22 57.40	18.17	56843	84					
12 52 59.42	-41 32 40.90	18.35			60746	158			
12 53 05.35	-41 42 39.90	15.85	27405	64					
12 53 17.38	-41 18 27.90	16.30	27937	63			27974		4
12 53 19.54	-41 19 01.00	17.83	9343	66					
12 53 19.88	-41 36 58.50	16.85	26216	81					
12 53 24.79	-41 17 58.80	16.70	27900	104			27913	27	4

<sup>a</sup>Total magnitudes from SExtractor(Bertin & Arnouts 1996)

<sup>b</sup>references: (1)Stein et al. (1997) (2)Dickens et al. (1986) (3)Mathewson & Ford (1996) (4)Stein (1996) (5)Smith et al. (2000) (6)Lauberts & Valentijn (1989) (7)de Vaucouleurs et al. (1991) (8)Bernardi et al. (2002) (9)Aguero et al. (1995)

Table 4. New Radial Velocities

$\alpha$ 2000.0	$\delta$	$V$ total <sup>a</sup>	$v_{rad}$ (Absorption)	Error	$v_{rad}$ (Emission)	Error
12 47 52.20	-41 20 13.60	18.05	2828*	88		
12 47 54.18	-41 03 44.90	15.56	4464	60		
12 47 55.84	-40 54 16.50	17.33	1817*	74		
12 48 07.29	-41 37 46.30	18.34	4188	106		
12 48 16.68	-41 26 10.60	17.34	2118	90		
12 48 48.56	-41 20 53.50	17.78	3053*	40		
12 50 22.00	-41 23 37.00	16.85	4450	77		
12 50 33.51	-41 20 09.80	16.31	2278	95		
12 50 34.63	-41 27 07.10	17.30	4608	128		
12 51 08.89	-41 40 12.30	16.25	2646	85		
12 52 02.38	-41 21 11.70	17.06	4327	68		
12 52 30.41	-40 55 43.10	15.69			2853*	37
12 52 32.86	-41 09 44.00	17.81			4553	44
12 52 35.13	-41 17 23.80	18.11			5059	113
12 52 42.58	-41 09 57.70	15.66	4333	36		

<sup>a</sup>Total magnitudes from SExtractor(Bertin & Arnouts 1996)

\*Galaxies are not included in the Centaurus Cluster Catalog (Jerjen & Dressler 1997)

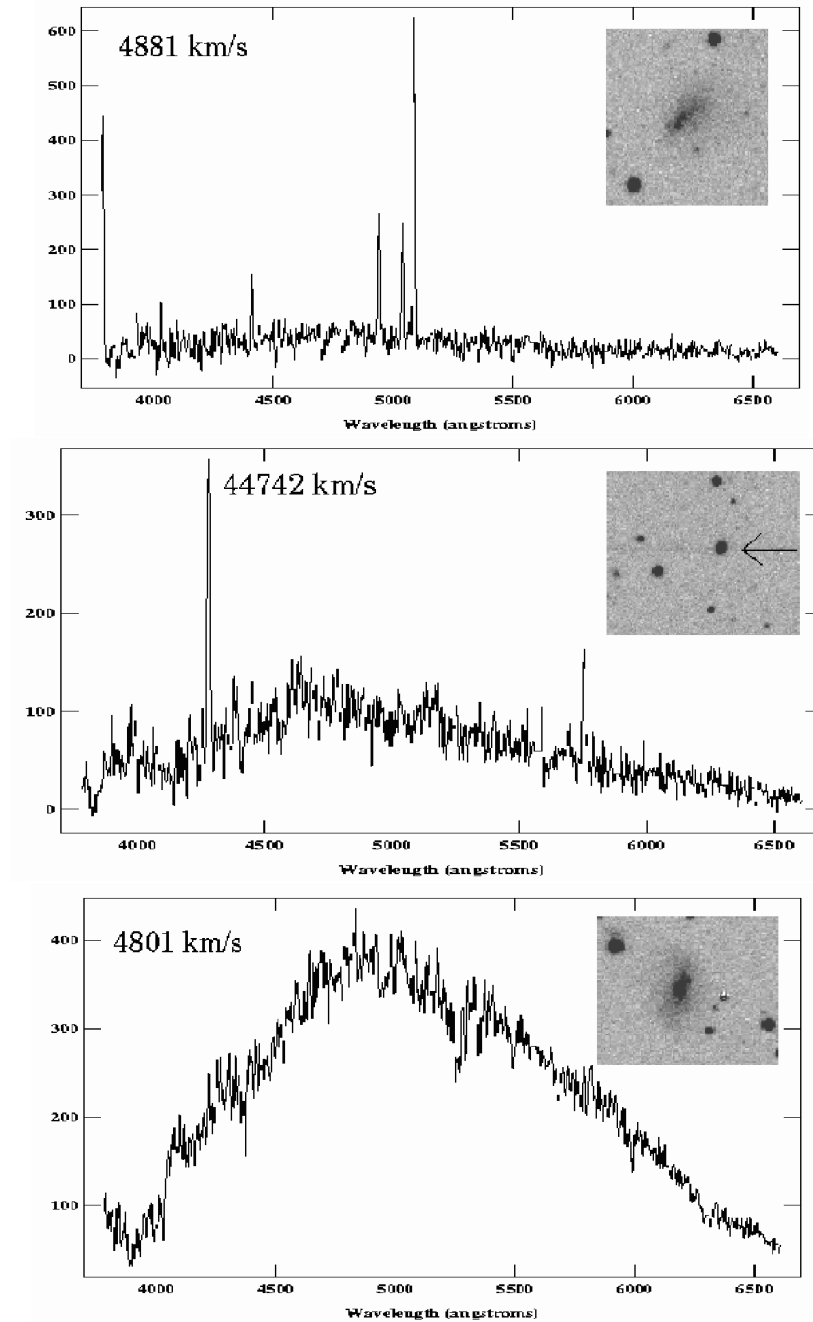


Fig. 1.— Spectra for three galaxies. The top and bottom plots display spectra of cluster dwarfs, while in the middle plot the compact, star-like object proved to be at high redshift. In the top plot, we were able to extract a redshift for the very LSB dwarf through its emission line spectrum. For the dwarf in the bottom plot, we obtained a redshift from cross correlation measurements of absorption lines due to the presence of a bright nucleus.

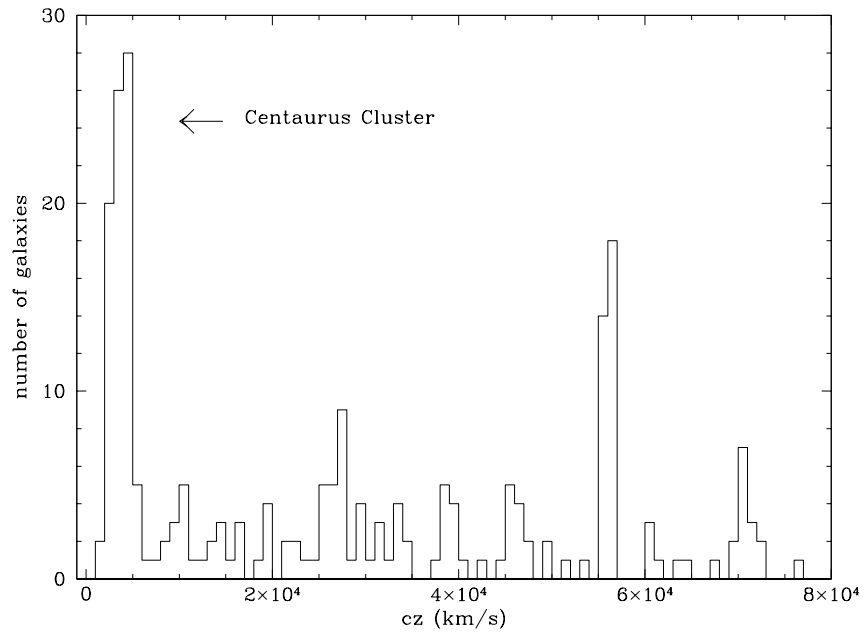


Fig. 2.— Histogram of the radial velocities obtained from the spectroscopic data. Several clusters or overdensities are evident behind Centaurus.

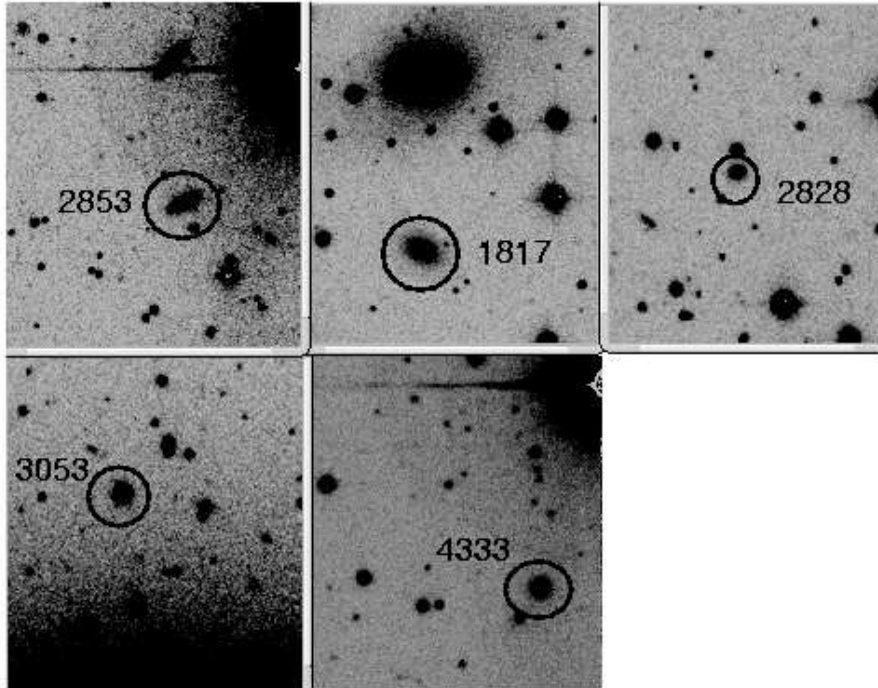


Fig. 3.— Five galaxies for which new redshifts have been obtained. Radial velocities (km/s) are printed next to the circled cluster dwarfs. All of these are likely Centaurus cluster members. While four of these (with the exception of the galaxy at 4333 km/s) are within the survey limits of the Centaurus Cluster Catalog of Jerjen & Dressler (1997), none are listed as members in the catalog.

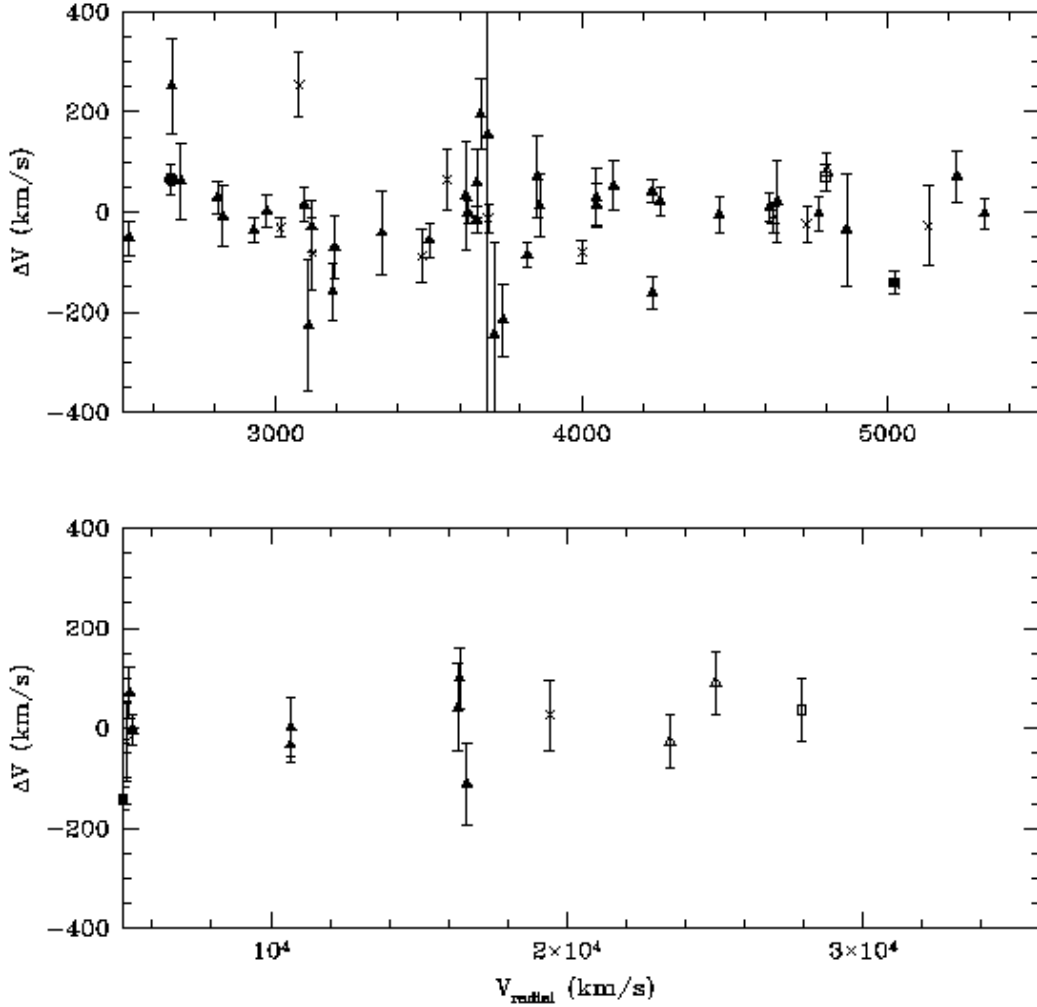


Fig. 4.— Comparison of radial velocities with literature values. We plot  $v_{\text{rad}}(\text{literature}) - v_{\text{rad}}(\text{this work})$  vs our radial velocity measurements. Solid triangles correspond to Stein et al. (1997), solid squares to Dickens et al. (1986), solid circles to Mathewson & Ford (1996), crosses to Stein (1996), open triangles to Smith et al. (2000), and open squares to Lauberts & Valentijn (1989).

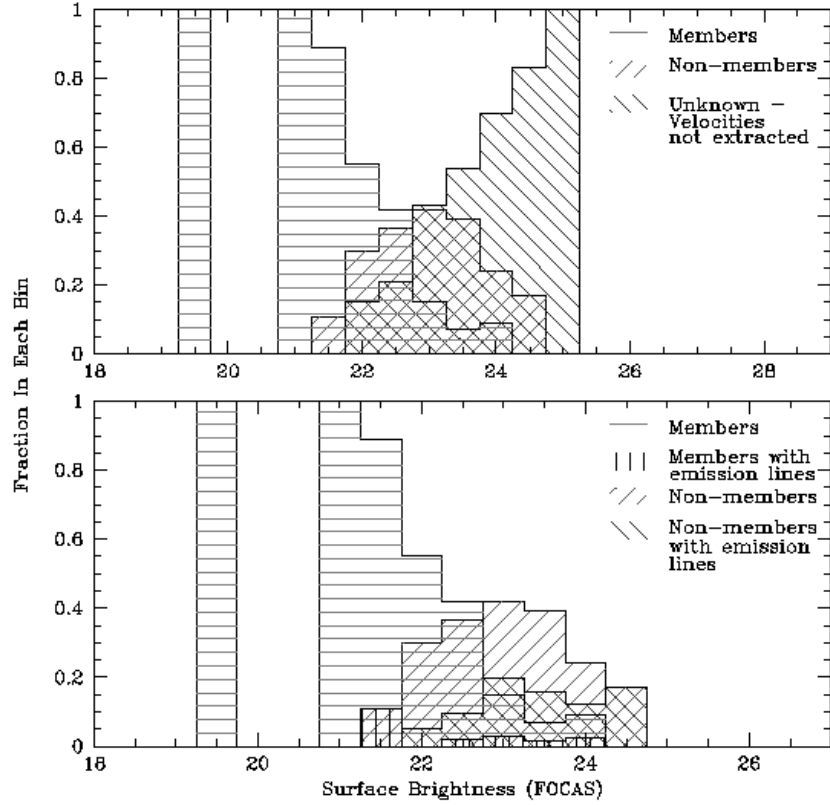


Fig. 5.— Centaurus cluster membership determined from spectra. We display the fraction in each surface brightness bin determined to be members or non-members. The surface brightness in this plot is the total surface brightness over the isophotal detection area. In the lower plot we further split detections into spectra with and without emission lines.

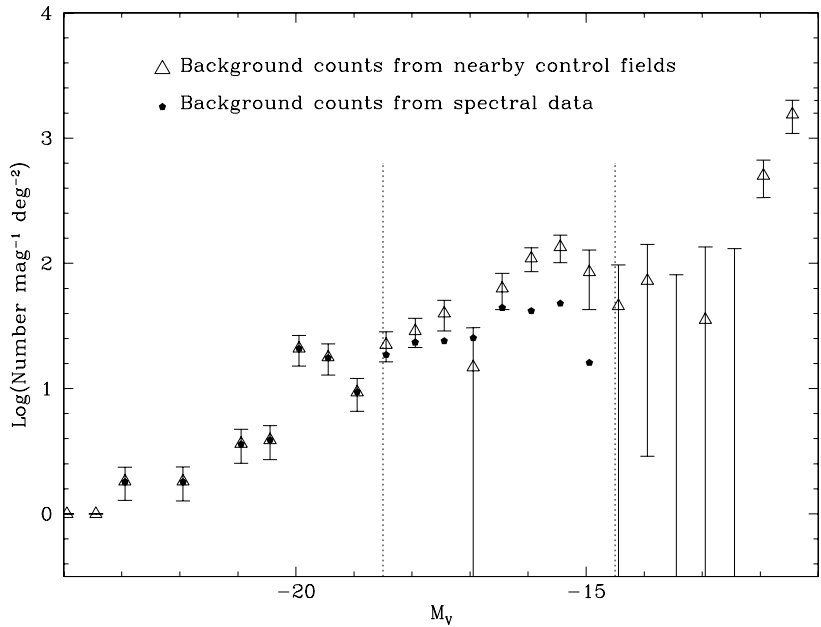


Fig. 6.— Centaurus cluster LF from spectroscopic results. Open triangles show cluster member counts after subtraction of local control field counts while solid symbols represent counts determined from redshifts. No correction is made for the spectra which did not yield redshift measurements. For clarity, error bars are only supplied for the former method. Neither spectra nor control field counts find background galaxies with  $V < 15$  (all galaxies brighter than  $M_V = -18.4$  are members), and member velocities were only obtained to  $M_V \sim -15.0$ .

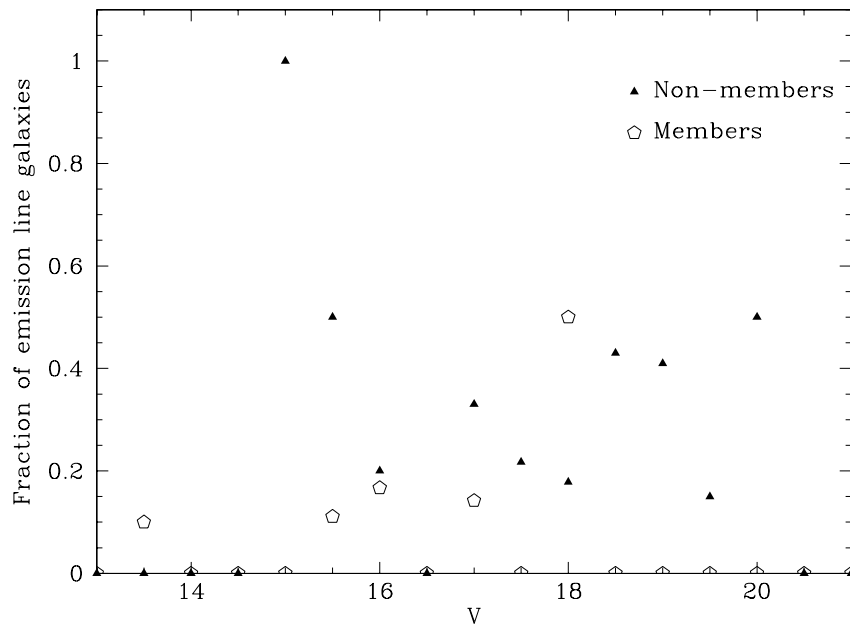


Fig. 7.— Fraction of galaxies with  $v_{rad}$  measured from emission line spectra in each half magnitude bin. Solid triangles represent the fraction of background galaxies with radial velocities determined from emission line spectra while open pentagons represent this fraction for cluster members.

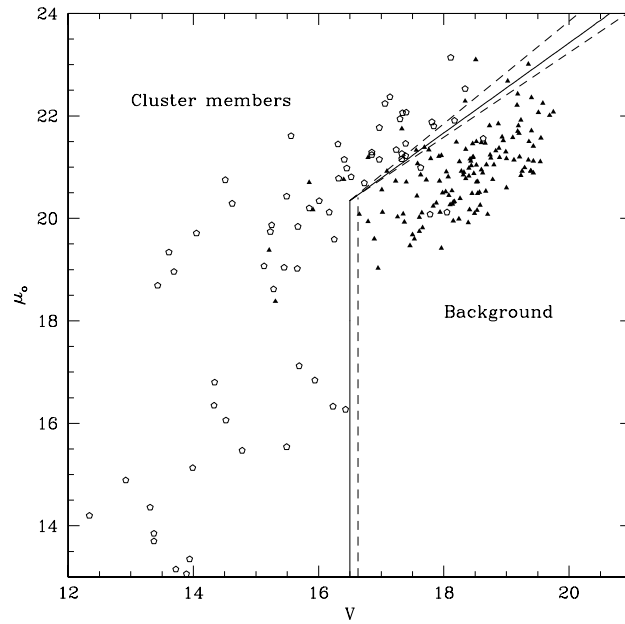


Fig. 8.— Central surface brightness vs. total magnitude for galaxies with measured redshifts. Open symbols represent cluster members while solid symbols indicate background galaxies. Lines are drawn which roughly separate these two populations. The solid lines define the surface brightness-magnitude criteria we use to determine membership. They are intentionally drawn to include as many member galaxies as possible. Dashed lines provide other possible delineations consistent with the data.

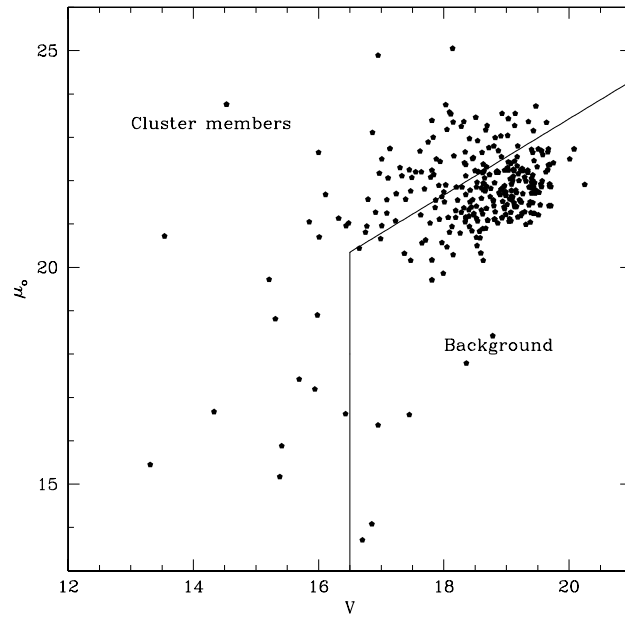


Fig. 9.—  $\mu_o$  vs.  $V$  for 306 galaxies for which redshifts were not obtained from the spectra. Note, the scale has been changed to include even lower surface brightness galaxies.

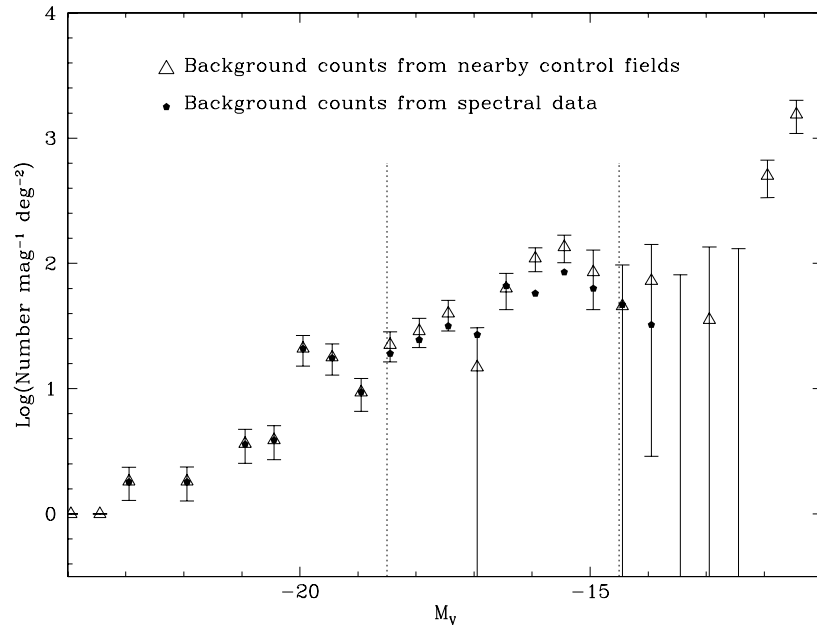


Fig. 10.— LF with correction for galaxies for which redshifts were not obtained. Again, the open triangles refer to member counts corrected by statistical background subtraction while the solid symbols are counts determined from spectra, now taking into account the 306 galaxies which did not produce measurable spectra.

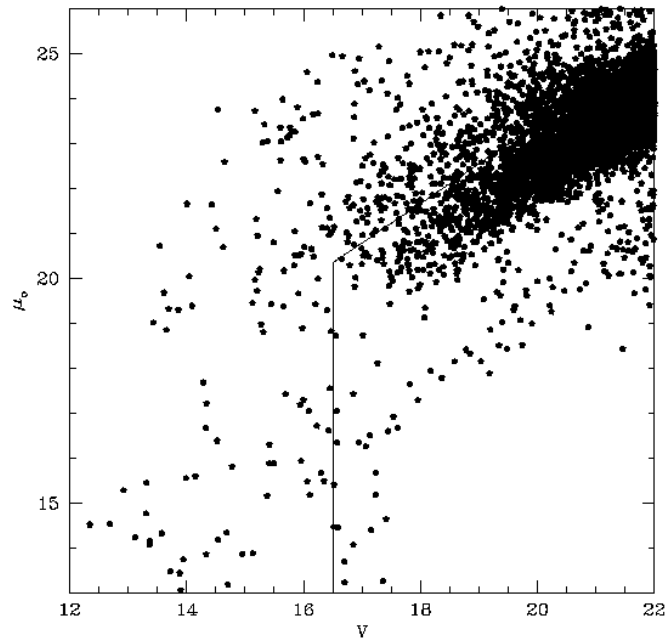


Fig. 11.—  $\mu_o$  vs.  $V$  for all galaxies within the central  $0.83 \text{ degrees}^2$  of the Centaurus cluster down to  $\mu_o = 26 \text{ mag / arcsec}^2$ . The lines separating the region of background from cluster galaxies are also displayed.

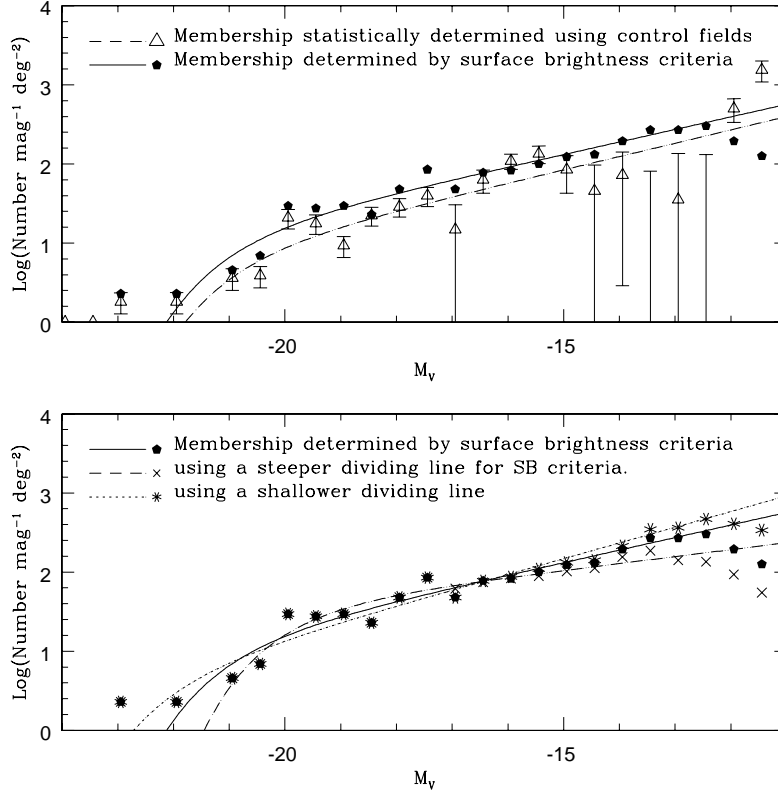


Fig. 12.— Centaurus cluster LF. Total counts are corrected for background contamination either with a statistical correction (open points), or through surface brightness-magnitude criteria (solid and skeletal points). In the upper plot, the dashed line is the best Schechter function fit ( $\alpha = -1.42 \pm 0.2$ ) for the statistical LF, while the solid line is the best fit for the surface brightness constructed LF, with  $\alpha = -1.40$ . In the lower plot, we test the effect of steepening and lowering the faint-end division line for this latter case and find the data are consistent with slopes as steep as  $-1.50$  and as shallow as  $-1.22$ . The fits only apply to  $V < 21$  ( $M_V < -12.4$ ).